PERGAMON

International Journal of Heat and Mass Transfer 42 (1999) 3509–3521

International Journal of HEAT and MASS TRANSFER

Analysis of local shellside heat and mass transfer in the shell-and-tube heat exchanger with disc-and-doughnut baffles

H. Li[a], V. Kottke[b,*]

[a]Jiangxi-OAI Joint Institute, Nanchang 330047, People's Republic of China
[b]Institute of Food Technology, Department of Food Process Engineering, Hohenheim University, 70599 Stuttgart, Germany

Received 15 April 1998; received in revised form 16 November 1998

Abstract

A mass transfer measuring technique is used to visualize and determine the shellside local heat transfer coefficients at each tube in two representative baffle compartments of a shell-and-tube heat exchanger with disc-and-doughnut baffles. The fluid flow adjacent to the tube is analysed and the heat transfer in the zones of separated flow discussed. The shellside flow distribution is determined through the measurements of the local pressure drop in the baffle-tube and baffle-shell clearances. Compared to the single-segmental baffle, the disc-and-doughnut baffles have a higher effectiveness of heat transfer to pressure drop. This investigation presents also per-tube and per-compartment averaged heat transfer coefficients.

Keywords: Shell-and-tube heat exchanger; Disc-and-doughnut baffle; Local heat transfer; Flow distribution; Mass transfer measuring technique

1. Introduction

The most widely used heat exchanger in industry is the shell-and-tube type, because of its relatively simple construction and multi-purpose application possibilities for gaseous and fluid media in a very large temperature and pressure range. For many years, various types of baffles have been used in shell-and-tube heat exchangers to improve heat transfer while maintaining a reasonable pressure drop across the exchanger. The most commonly used baffle, the segmental baffle, causes the shellside fluid to flow across the tube bundle. This improves heat transfer by enhancing turbulence or local mixing on the shell side of the exchanger, but at the cost of a high pressure drop. This is caused by flow separation at the edge of the baffles with subsequent flow contraction and expansion. Due to its broad application, a lot of work has been reported in this field [1–13].

Compared to segmental baffles, disc-and-doughnut baffles have not achieved similar popularity, mainly because of manufacturing problems and the absence of comparable information on heat transfer and pressure loss [14]. They have higher effectiveness of heat transfer to pressure drop than segmental baffles [1,14–16], which is due to the radial flow between the bundle centre and periphery, which eliminates bundle bypass, and uses much lower cross-flow mass velocity than segmental baffles [14].

In this investigation, the shellside local heat transfer

* Corresponding author. Tel.: +49-711-459-3258; fax: +49-711-459-3443.

0017-9310/99/$ - see front matter
PII: S0017-9310(98)00368-8

Nomenclature

a	pitch ratio, $a = s_1/d$
b	surface mass density [kg/m^2]
A	flow area, $A = D_i S$ [m]
d	tube outside diameter [m]
D_i	inside diameter of the shell [m]
l	characteristical length, $l = \pi d/2$ [m]
L	distance of two baffle compartments [m]
$\dot{m}_a$	density of mass flow rate [kg/m^2 s]
M_a	mass of gas injected into the air stream [kg]
Nu	Nusselt number
ΔP	pressure drop of two compartments [N/m^2]
Pr	Prandtl number
Re	Reynolds number
S	baffle spacing [m]
s_1	tube pitch cross [m]
Sc	Schmidt number
Sh	Sherwood number
t_v	experimental time [s]
$\dot{V}$	inlet flow rate [m^3/s]
X	tube length [m].

Greek symbols

α	heat transfer coefficient [W/(m^2 K)]
β_a	mass transfer coefficient [m/s]
λ	thermal conductivity [W/(K m)]
ρ	density [kg/m^3]
ν	kinematic viscosity [m^2/s].

Subscripts

a	ammonia
w	wall
∞	in main stream.

coefficients of a shell-and-tube heat exchanger with disc-and-doughnut baffles are measured by applying a mass transfer measuring technique which is based on absorption, chemical and colour giving reaction [17–19]. The visualization of the local shellside heat transfer coefficient by mass transfer at the individual tubes gives information on the local fluid flow adjacent to the surface of each tube. Through measurements of pressure drop in the baffle-shell and the baffle-tube clearances, local shellside flow distributions are calculated for different inlet flow rates. The results in this paper allow the formulation and appraisal of prediction methods and, as a result, improve current design of the shell-and-tube heat exchangers with disc-and-doughnut baffles. The development of the local heat transfer coefficients in the stagnation regions will be discussed, which is important for the improvement of the integral heat exchanger and for reduction of fouling in these regions.

In order to compare the effectiveness of heat transfer to pressure drop for different baffle types, the ratio of the integral shellside heat transfer coefficients to pressure drop for single-segmental baffle and disc-and-doughnut baffle will be presented.

2. Experimental apparatus and procedure

The experimental shell-and-tube heat exchanger model consists of a cylindrical plexiglass shell (1) and two removable PVC tube sheets (2), which support a bundle of glass tubes (3) and six tie rods (4). Fig. 1 shows the internal configuration with a staggered tube arrangement in the test section. Each tube location is denoted by two numbers, the first of these is the number of the row from top to bottom, where the tube is located. The second number indicates the tube position within the row from left to right. Only tubes at the

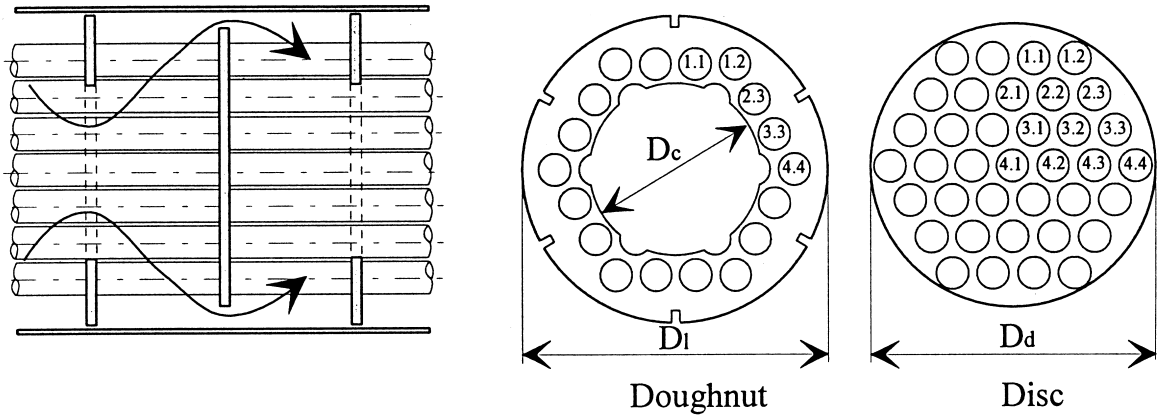

Fig. 1. Internal configuration of experimental heat exchanger.

right side are denoted, because of the symmetric tube arrangement. All of the tubes were made removable and can be replaced by a mass transfer measuring tube (Fig. 2a) or by a pressure sensing tube (Fig. 2b). The essential dimensions and features of the heat exchangers are given in Table 1.

The experimental apparatus is shown in Fig. 3. Air is induced into the equipment by a fan, while the flow velocity is measured with a Bellmouth intake and Betz pressure gauge. A mixer produces a uniform profile of the tracer gas (ammonia) and the flow is homogenized through a honeycomb. The test section is located in the third and fourth baffle compartments from the exchanger inlet, which are in the fully developed flow region.

For the visualization and mass transfer measurements, the outer surface of the mass transfer measuring tube is coated with a wet filter paper containing an aqueous solution of manganese(II)chloride with hydrogenperoxide as shown in Fig. 2a. This measuring tube is then inserted in the heat exchanger. A defined quantity of reaction gas NH_3 is added in given quantity to the main stream in a very low concentration. Due to its unique solubility, it is absorbed quantitatively in the wet filter paper according to local partial concentration differences. After absorption, the following reactions take place:

$$NH_3 + H_2O \rightleftharpoons NH_4^+ + OH^-$$

$$2NH_4OH + MnCl_2 \rightarrow 2NH_4Cl + Mn(OH)_2$$

$$Mn(OH)_2 + H_2O_2 \rightarrow MnO_2\downarrow + 2H_2O.$$

The colour intensity of manganese dioxide indicates directly the locally transferred mass and can be evaluated quantitatively by photometrical remission processing [17,18].

The mass rate transferred to the surface is described by

$$\dot{m}_a = \beta_a(\rho_{a\infty} - \rho_{aw}) \tag{1}$$

for the condition that the reacting gas component is added as a pulse

$$\int_{t=0}^{t_v} \dot{m}_a \, dt = \int_{t=0}^{t_v} \beta_a \rho_{aw} \, dt \quad \text{with } \rho_{aw} = 0 \tag{2}$$

where

$$\int_{t=0}^{t_v} \dot{m}_a \, dt = b$$

is the 'surface mass density' b, that means the total amount of mass transferred to the unit area of the surface. Integration of the right hand side of Eq. (2) gives

$$b = \beta_a M_a / \dot{V} \tag{3}$$

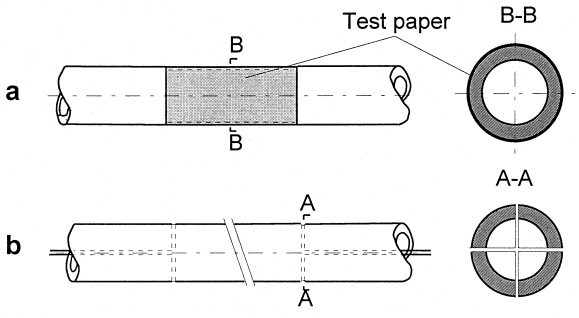

Fig. 2. Measuring tube for mass transfer (a) and pressure drop (b).

Table 1
Main dimensions and features of experimental heat exchanger

Item	Dimensions and description (mm)	Item	Dimensions and description
Inside diameter of shell [D_i]	290	Pitch ratio	1.26
Diameter of tubes [d]	30	Baffle type	Double-segmental
Doughnut outer diameter [D_1]	286	Number of tubes	37
Doughnut-hole diameter [D_c]	163	Baffle spacing S	113
Disc diameter [D_d]	264	Tube arrangement	Staggered

$$\beta_a = \frac{b\dot{V}}{M_a} \tag{4}$$

where $\dot{V}$ is the constant air flow rate and M_a the total amount of gas added with the pulse. The problem of determining local mass transfer is reduced to

- determining the total mass M_a of added gas;
- measuring of colour density distribution for evaluation of surface mass density b; and
- coating any given surface with very thin layers, which contain all surface side reaction components and which remain wet even at very high velocity and very thin-film thickness.

This mass transfer measuring technique is applicable for both developable and undevelopable surfaces. It is characterized by simple handling, good local accuracy and high resolution. The reaction system is not toxic in the used concentration, which makes the application in open and closed wind tunnels on an industrial scale possible [18]. This mass transfer measuring method corresponds to an isothermal surface in the heat transfer application. The analysis of the local or integral heat and mass transfer at a single active tube at each time has the big advantage that the boundary conditions, especially the concentration or temperature, in the fluid are exactly known. If the whole tube bundle is active, the concentration or temperature in the fluid cannot be exactly determined depending on the limited mixing on the wake of the cylinders. Therefore, the determination of local or integral heat and mass transfer at a single tube in the tube heat exchanger allows a more accurate access, as long as the flow is not changed by the effects of free convection.

The conversion from mass transfer data into heat transfer data is based on the extended Lewis analogy

$$\frac{Nu}{Sh} = \frac{Pr^{n_1}}{Sc^{n_2}} \tag{5}$$

The exponents n_i are in the range between ($Pr \to \infty$) $0.33 \leqslant n \leqslant 0.5$ ($Pr \to 0$) for laminar boundary layers and ($Pr \to \infty$) $0.33 \leqslant n \leqslant 1.0$ ($Pr \to 0$) for turbulent boundary layers [17]. For the used mass transfer measuring technique, the Schmidt number is $Sc = 0.616$, and for

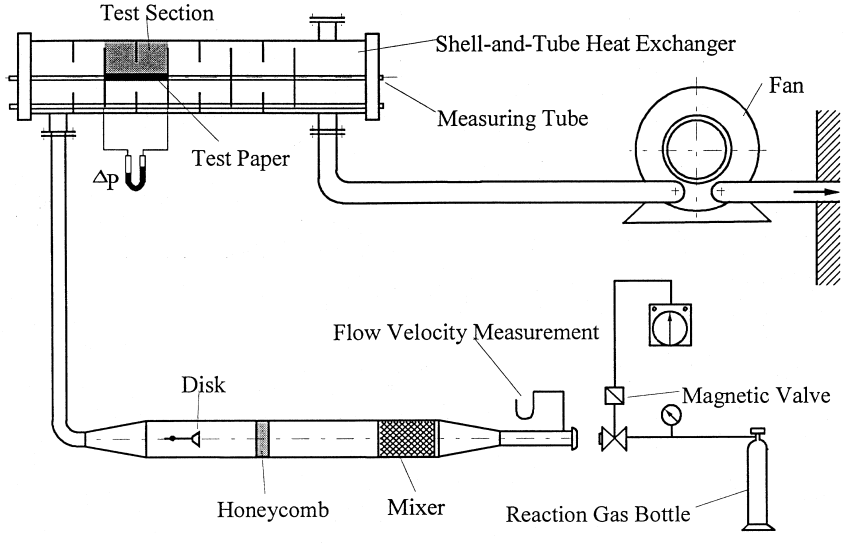

Fig. 3. Schematic diagram of experimental apparatus.

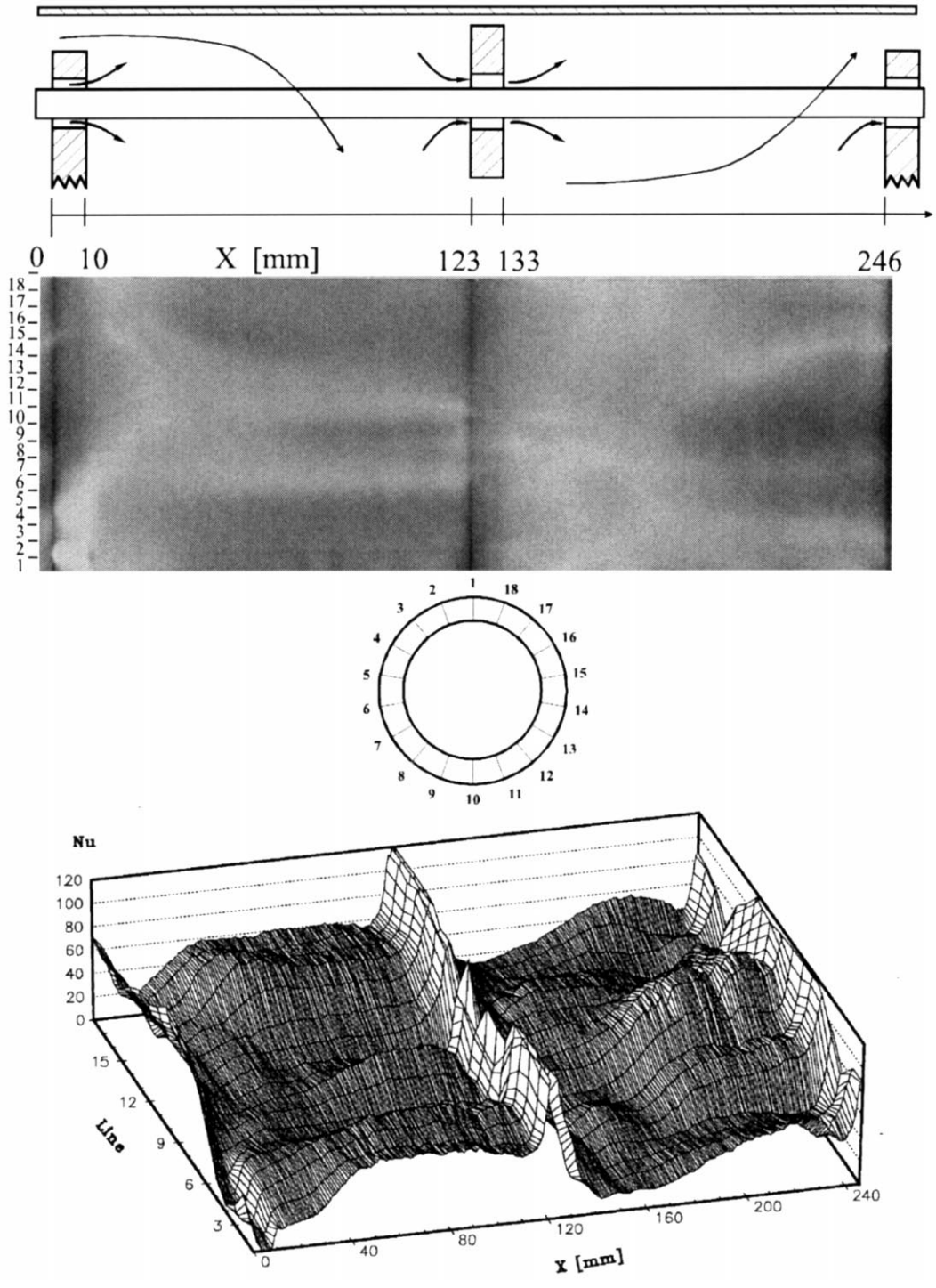

Fig. 4. Visualization and distribution of local mass and heat transfer at the surface of the tube 1.1 for $Re = 8000$.

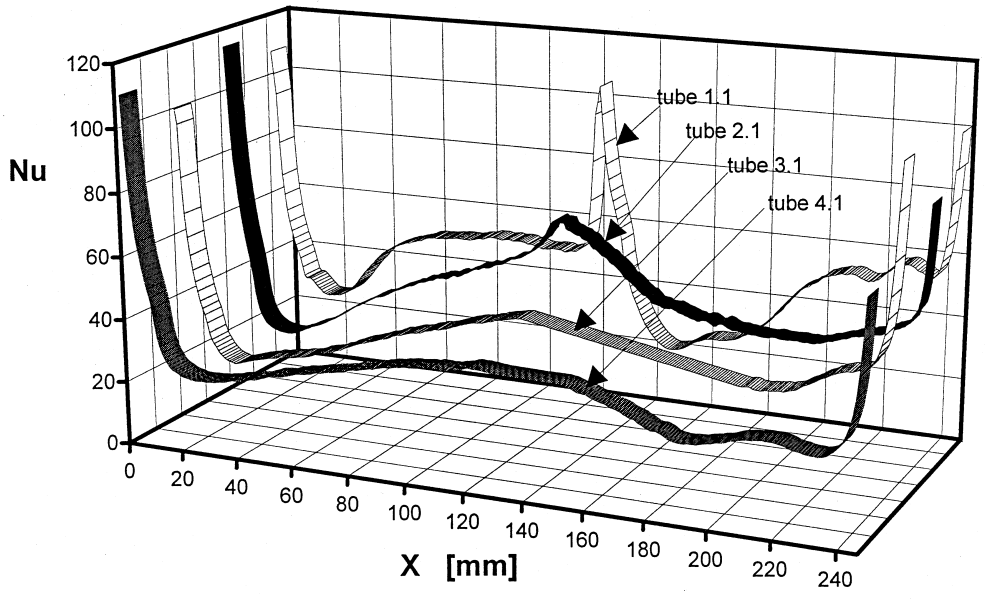

Fig. 5. Longitudinal profiles of local Nusselt number averaged over the tube circumference at tubes 1.1, 2.1, 3.1 and 4.1 for $Re = 8000$.

the heat transfer in air the Prandtl number is $Pr = 0.712$. As the Schmidt number here is close to the Prandtl number, $n_1 = n_2 = 0.37$ for laminar boundary layers and $n_1 = n_2 = 0.6$ for turbulent boundary layers, the conversion equation for laminar as well as turbulent boundary layers is then for $Sc = 0.61$ and $Pr = 0.71$

$$Nu = 1.07Sh \tag{6}$$

The mass transfer measurements (Sherwood numbers) have an uncertainty of about $\pm 3\%$ depending on the photometric measurements and calibration [17–19]. The uncertainty of the calculation of heat transfer from mass transfer coefficient using Eq. (6) is $\pm 2\%$. This uncertainty includes that laminar and turbulent boundary layers are handled with a mean factor of 1.07 instead of 1.05 for laminar, and 1.09 for turbulent boundary layers.

The uncertainty on pressure coefficients is about 5% at low flow velocity ($Re < 1000$) and about 3% at high flow velocity ($Re \geqslant 1000$). Reynolds numbers are calculated with the volume flow through a Bellmouth intake, which has an uncertainty of $\pm 2\%$.

The Reynolds number is defined according to VDI-Wärmeatlas [20]

$$Re = \frac{\pi d \dot{V}}{2(1 - \pi/4a)D_i S \nu} \tag{7}$$

It should be noted that this definition is based on the velocity in the cross-flow zone of the shell-and-tube heat exchanger with single-segmental baffles. For the heat exchangers with double-segmental baffles, the baffles split the flow into two parallel streams which flow in a zigzag manner to the tube bundle. It therefore follows that for the same inlet volumetric flow rate and the same baffle spacing, double-segmental baffles will give considerably lower velocity in the cross-flow zone than single-segmental baffles. In order to simplify the comparison of the two baffles types, this definition is still used in this paper.

3. Results and discussion

3.1. Local mass and heat transfer

Fig. 4 shows a representative sample of the local mass and heat transfer distribution at the surface of the tube 1.1 for $Re = 8000$. The photograph illustrates the distribution of the local transferred mass. The corresponding distribution of the local heat transfer is given at the bottom, where the axis X is the tube length in the test section (third baffle compartment $X = 0$–123 mm and fourth baffle compartment $X = 123$–246 mm) and y-axis line is the angular location as shown in this figure. From $X = 0$–10 mm, the local mass and heat transfer distribution in the baffle-tube clearance between the tube and a disc baffle is presented. The high local Nusselt numbers at $X = 0$ mm are due to the thin boundary layer in the annular ori-

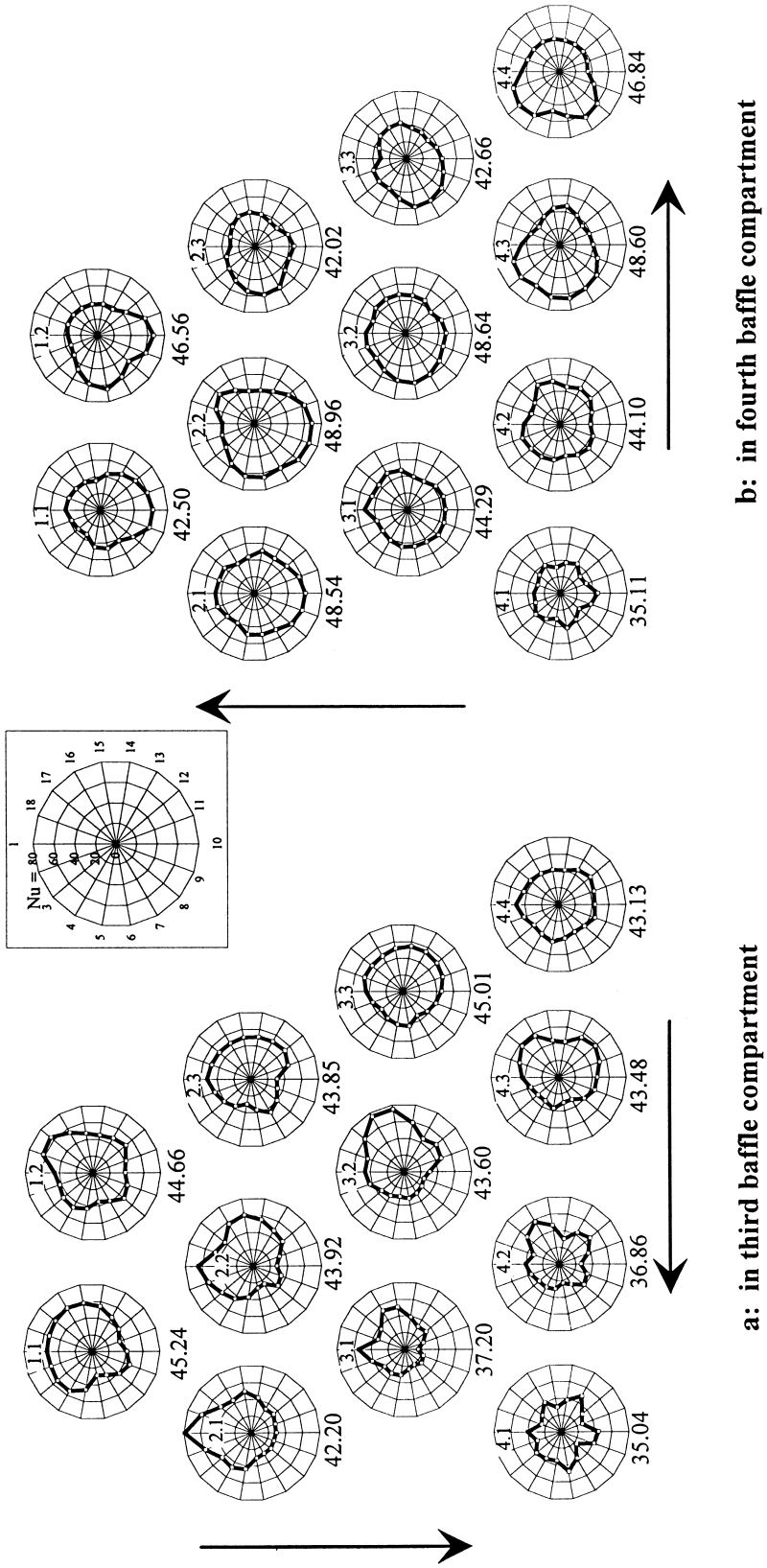

Fig. 6. Circumferential distribution of local Nusselt number averaged over tube length for $Re = 8000$.

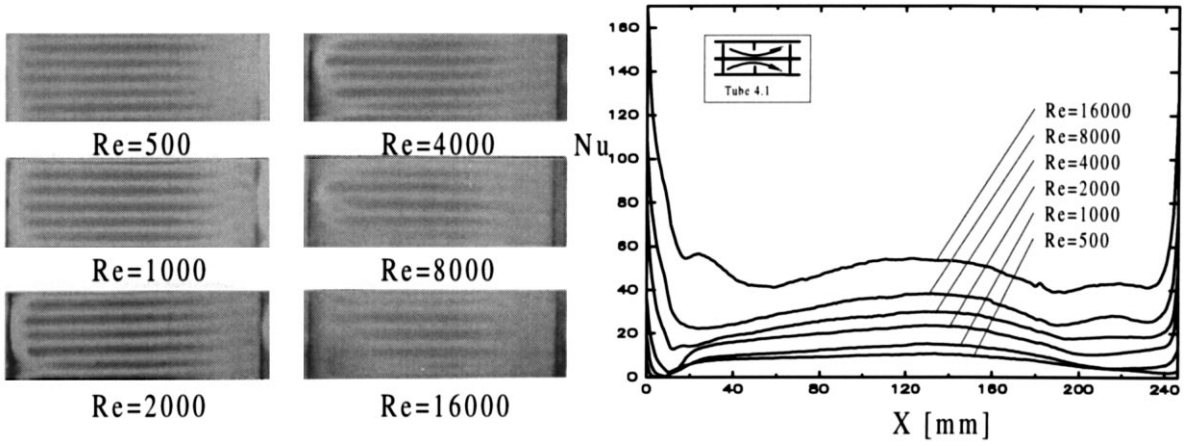

Fig. 7. Distribution of local mass and heat transfer at the tube 4.1.

fice entrance. The lower mass and heat transfer behind the disc baffle ($X=10$–30 mm) reveals a stagnation region. A similar distribution of the mass and heat transfer as that from $X=0$–10 mm appears from $X=123$–133 mm in the baffle-tube clearance between the tube and a doughnut baffle. Behind the doughnut baffle ($X=133$–183 mm), there is a zone of separated flow with lower mass and heat transfer coefficients. From $X=183$–246 mm, the fluid flows across the tube, where the front stagnation line with higher local mass and heat transfer coefficients at line 10 can be seen.

During the optimization of the heat exchangers

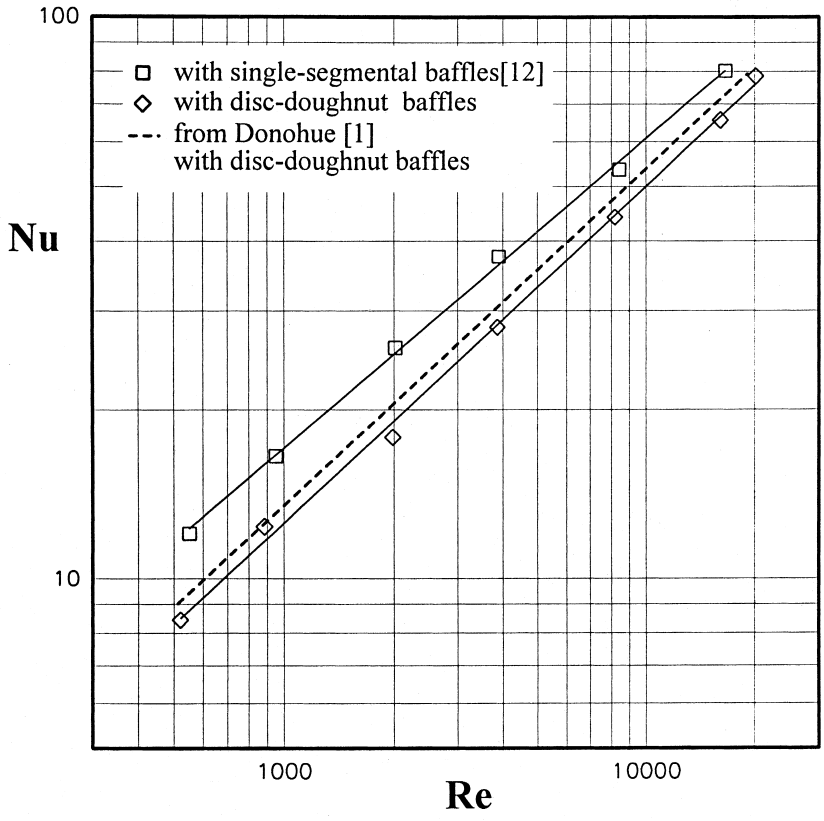

Fig. 8. Averaged Nusselt number in the test baffle compartments.

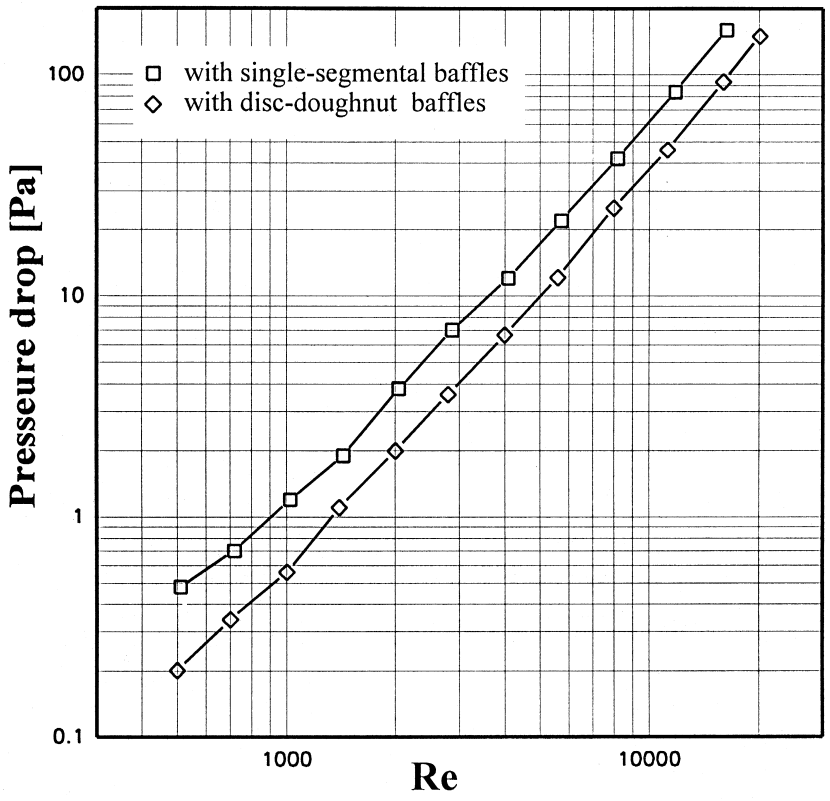

Fig. 9. Pressure drop in two baffle compartments.

with baffles, improvement of the heat transfer and reduction of the fouling in the zone of separated flow should be considered. In this case, a detailed information about the local heat transfer coefficients and about the flow field in the baffle compartments is useful. In Fig. 5, the profiles of the Nusselt number averaged over the tube circumference at tubes 1.1, 2.1, 3.1 and 4.1 show the size of the zone of separated flow behind the disc-and-doughnut baffles. The tube length (x-axis) in this figure is defined as in Fig. 4. The flow separation at the edge of the disc baffle results in a large zone of separated flow which increases from tube 1.1 to tube 4.1. The heat transfer coefficients there are obviously lower than in other regions. Behind the doughnut baffle, the weak recirculation in the local separated flow [21] is the reason for the remarkable variation of the heat transfer at tube 1.1 from $X=133$ mm to $X=200$ mm.

Fig. 6 shows the circumferential distribution of the local Nusselt number averaged over each tube length in the third (Fig. 6a) and the fourth baffle compartment (Fig. 6b) for $Re=8000$. Depending on the symmetric tube arrangement, only the distributions at the tubes from rows 1–4 are given. The arrows in this figure identify the direction of the external flow through the tube bundle. The per-tube averaged Nusselt numbers are also given in this figure. One noteworthy feature in this figure is that the variation of the per-tube averaged Nusselt number from tube to tube is not noticeable, except the lower heat transfer at tubes 3.1, 4.1 and 4.2 in Fig. 6a and at tube 4.1 in Fig. 6b. Another feature in this figure is the similar circumferential distribution at the symmetric tubes, e.g. tubes 1.1 and 3.3, tubes 1.2 and 4.4, and tubes 2.1 and 3.2. The similarity of the distribution at these symmetric tubes in Fig. 6a depends on the strong recirculation flow behind the disc baffle [21], as also shown in Fig. 6b. The circumferential distributions of the heat transfer in this figure also reveal the shellside flow field.

Fig. 7 shows the mass and heat transfer distribution for $Re=500$–16,000 at tube 4.1 which is located in the centre of the tube bundle. The fluid flows over the edge of the disc baffle and is turned into the tube bundle by the subsequent doughnut. It flows almost parallel to the tube bundle through the hole of the doughnut baffle and is then turned in the radial direction by the subsequent disc baffle. The photograph of the mass transfer distribution in Fig. 7a indicates that

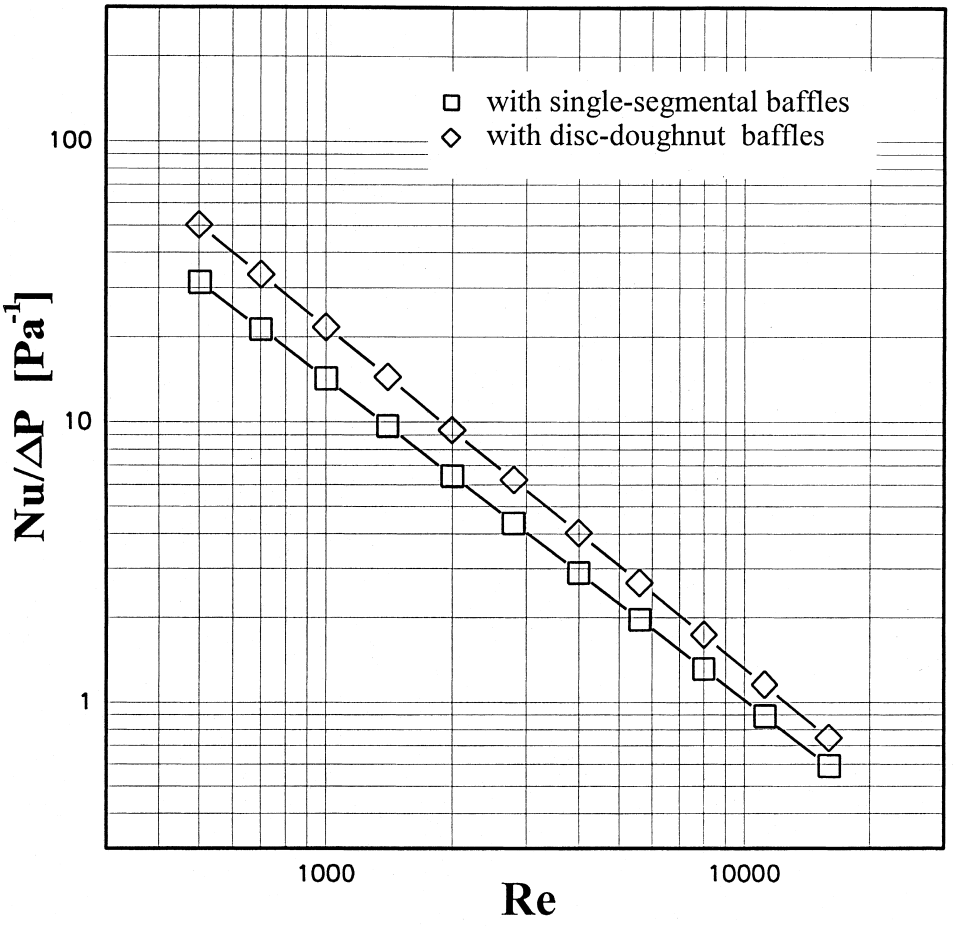

Fig. 10. Ratio of heat transfer to pressure drop.

six longitudinal vortices (Taylor–Goertler vortices) develop symmetrically around the tube. They correspond to the six gaps formed by the adjacent six tubes (see Fig. 1). These longitudinal vortices are destroyed by the turbulence of higher Reynolds number ($Re > 8000$). It is worth noting, that the effective Reynolds number, based on the local real flow velocity, is much smaller. The profiles of the Nusselt number averaged over the tube circumference in Fig. 7b are almost parallel for $Re = 500$–$16{,}000$. An exception is in the stagnation region behind the disc baffle ($X = 10$–60 mm) where the heat transfer can be obviously improved by an increase of the Reynolds number, depending on the recirculation flow.

3.2. Integral heat transfer and pressure drop

The averaged Nusselt numbers in the test baffle compartments are plotted as a function of the Reynolds number in Fig. 8. It is calculated for $Re = 1000$ and $Re = 8000$ from the determined local heat transfer coefficients at each tube of the tube bundle (an example is presented in Fig. 6) and for the other Reynolds numbers from the values at four chosen representative tubes 1.1, 2.1, 3.1 and 4.1. This figure shows a good agreement between the results in this investigation and the predicted values according to Donohue [1,22,23]. The Reynolds number defined by Donohue is converted.

For comparison of the effectiveness of heat transfer to pressure drop for different baffle types, Figs. 8 and 9 give the per-compartment averaged heat transfers and the pressure drop in two baffle compartments (Fig. 3) in the shellside of the heat exchangers, which have the same internal configuration, with the exception of the baffle type [10–12]. For the same Reynolds number, they have the same inlet volumetric flow rate. The heat transfer for disc-and-doughnut baffles is about 78% of that for single-segmental baffles as shown in Fig. 8, because of the lower flow velocity for disc-and-doughnut baffles. The pressure drop for disc-and-doughnut baffles is however only about 55% of

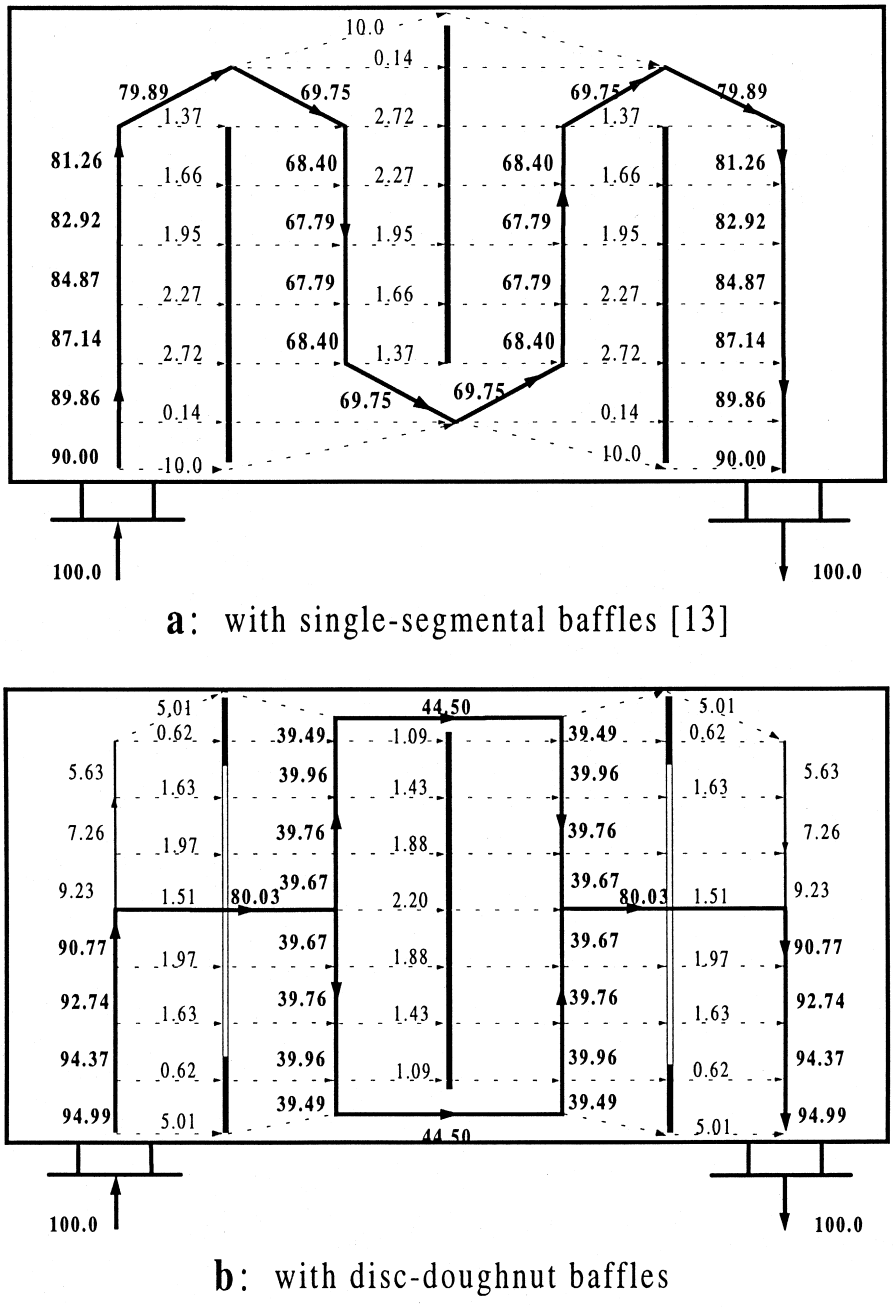

Fig. 11. Flow distribution relative to the inlet volumetric flow rate for $Re = 8000$.

that for single-segmental baffles. The ratio of the per-compartment averaged heat transfer to the pressure drop for the two baffle types is plotted as a function of the Reynolds number in Fig. 10. The effectiveness of the heat exchanger with disc-and-doughnut baffles is obviously higher than that for single-segmental baffles. This result agrees with the reports from Donohue [1] and Sharif [16].

3.3. Flow distribution

The fluid velocity u_0 through either the baffle-shell

clearance or the baffle-tube clearance can be calculated from

$$u_0 = \sqrt{\frac{2\Delta P_2}{\rho \zeta_0}} \tag{8}$$

if the pressure drop ΔP_2 due to flow through these clearances and the pressure drop coefficient ζ_0 are known. According to Kukral [9], ζ_0 depends primarily on the orifice Reynolds number Re_0 and the orifice shape factor Z

$$\zeta_0 = f(Re_0, Z) \tag{9}$$

$$Re_0 = w_0(D-d)/\nu \tag{10}$$

$$Z = 2\delta/(D-d), \tag{11}$$

where D and d denote outer and inner diameter of the annular orifices in a plate of thickness δ. By this investigation, the pressure drop in the baffle-shell and baffle-tube clearances is measured.

In Fig. 11 the local percentages of the main stream and of the leakage streams are given relative to the inlet volume flow rate for single-segmental baffles [13] and disc-and-doughnut baffles. In the heat exchanges with disc-and-doughnut baffles the baffle-shell leakage exists only in the clearances between the shell and the doughnut baffles. This leakage gives almost no contribution to heat transfer [12]. The percentage of the baffle-shell leakage for single-segmental baffle is twice the value of that for disc-and-doughnut baffles for $Re = 8000$. The percentage of the main stream for single-segmental baffles is therefore lower than that for disc-and-doughnut baffles. This is one of the reasons why the disc-and-doughnut baffles have a higher effectiveness of heat transfer to pressure drop than single-segmental baffles.

4. Conclusions

A mass transfer measuring technique is used in this investigation to visualize and determine the shellside distribution of the heat transfer coefficients at each tube surface in two representative baffle compartments of a shell-and-tube heat exchanger with disc-and-doughnut baffles, which reveals the flow field, particularly the size of the stagnation behind the baffles. The low heat transfer in this stagnation region can be considerably improved through the recirculating flow for high Reynolds number. Longitudinal vortices (Taylor–Goertler vortices) are observed in the centre of the tube bundle for $Re = 500$–$16{,}000$. The disc-and-doughnut baffles have a higher effectiveness of heat transfer to pressure drop than single-segmental baffles because of partly a lower percentage of baffle-shell leakage. The detailed knowledge about the shellside local heat transfer coefficients and about the flow distribution provided in this investigation allows a further improvement of the shell-and-tube heat exchangers.

References

[1] D.A. Donohue, Heat transfer and pressure drop in heat exchangers, Industrial and Engineering Chemistry 41 (1949) 2499–2511.

[2] T. Tinker, Shell side characteristics of shell and tube heat exchanger, Parts I, II and III, General Discussion on Heat Transfer, The Institution of Mechanical Engineers, London, 1951, pp. 89–116.

[3] K.J. Bell, Final Report of the Cooperative Research Program on Shell and Tube Heat Exchangers, University of Delaware Engineering Experimental Station, Bulletin No. 5, 1963.

[4] B. Gay, T.A. Williams, Heat transfer on the shell-side of a cylindrical shell-and-tube heat exchanger fitted with segmental baffles—I. Bundle and zonal average heat transfer coefficients, Trans. Instn. Chem. Engrs. 46 1968 T95–T100.

[5] J.W. Palen, J. Taborek, Solution of shell side flow pressure drop and heat transfer by stream analysis method, Chem. Eng. Progr. Symp. Ser. 92 (1969) 53–63.

[6] B. Gay, N.V. Mackley, J.D. Jenkins, Shell-side heat transfer in baffled cylindrical shell-and-tube exchangers—an electrochemical mass transfer modelling technique, Int. J. Heat Mass Transfer 19 (1976) 995–1002.

[7] E.M. Sparrow, J.A. Perez, Internal shell-side heat transfer and pressure drop characteristics for a shell-and-tube heat exchanger, J. Heat Transfer 107 (1985) 345–353.

[8] W. Roetzel, Y. Xuan, Dispersion model for divided-flow heat exchanger, in: Proceedings of the EUROTHERM Seminar No. 18, Hamburg, 1991, pp. 98–110.

[9] R. Kukral, K. Stephan, The effect of internal leakage on steady-state and transient behaviour of shell-and-tube heat exchangers, in: Proceedings of the 10th International Heat Transfer Conference, Brighton, UK, 1994, pp. 393–398.

[10] H.D. Li, Strömungs- und Transportvorgänge in Rohrbündelwärmeübertragern, VDI-Fortschritt Berichte, Reihe 7, No. 316, VDI-Verlag, Düsseldorf 1997.

[11] H.D. Li, V. Kottke, The effect of baffle-tube leakage on the local mass and heat transfer in the shell-side of shell-and-tube heat exchangers, J. Flow Visualization and Image Processing 4 (1997) 129–139.

[12] H.D. Li, V. Kottke, Effect of the leakage on pressure drop and local heat transfer in shell-and-tube heat exchangers for staggered tube arrangement, Int. J. Heat Mass Transfer 41 (2) (1998) 425–433.

[13] H.D. Li, V. Kottke, Effect of baffle spacing on pressure drop and local heat transfer in shell-and-tube heat

exchangers for staggered tube arrangement, Int. J. Heat Mass Transfer 41 (10) (1998) 1303–1311.
[14] J. Taborek, Selected problems in heat exchanger design, in: Proceedings of the EUROTHERM Seminar No. 18, Hamburg, 1991, pp. 3–18.
[15] F. Ratnasamy, Exchanger design using disc-and-doughnut baffles, Hydrocarbon Processing 66 (4) (1987) 63–65.
[16] A. Sharif, D. Klein, J.R. Howell, Effectiveness of pressure drop to heat transfer conversion for various shell-side flow configurations, ASME/JSME Thermal Engineering Proceedings 4 (1991) 439–448.
[17] V. Kottke, H. Blenke, K.G. Schmidt, Eine chemische Farbreaktion zur Messung örtlicher Stoffübertragung und Sichtbarmachung von Strömungsvorgängen, Wärme- und Stoffübertragung 10 (1977) 9–21.
[18] V. Kottke, A chemical method for flow visualization and determination of local mass transfer, flow visualization—II, in: Proceedings of the Second International Symposium on Flow Visualization, 9–12 September, Bochum, Germany, 1980, pp. 657–662.
[19] V. Kottke, H. Blenke, K.G. Schmidt, Messung und Berechnung des örtlichen und mittleren Stoffübergangs an stumpf angeströmten Kreisscheiben bei unterschiedlicher Turbulenz, Wärme- und Stoffübertragung 10 (1977) 89–105.
[20] E.S. Gaddis, V. Gnielinski, Wärmeübertragung im Außenraum von Rohrbündel-Wärmeübertragern mit Umlenkblechen, VDI-Wärmeatlas, 6. Aufl., VDI-Verlag, Düsseldorf, Abschnitt Gg 1–6 1991.
[21] M.A. Founti, C. Vafidis, J.H. Whitelaw, Shell-side distribution and the influence of inlet conditions in a model of a disc-and-doughnut heat exchanger, Experiments in Fluids 3 (1985) 293–300.
[22] B. Slipcevic, Auslegung von Wärmeübertragern mit Kreisscheiben und -ringen, Technische Rundschau Sulzer 58 (3) (1976) 114–120.
[23] B. Slipecevic, Druckabfall im Mantelraum von Rohrbündel-Wärmeübertragern mit Kreisscheiben und -ringen, Technische Rundschau Sulzer 60 (1) (1978) 28–30.